Design and Simulation of Long Baseline Navigation Systems

Tiago Filipe Nunes da Silva
tiago.filipe.silva@tecnico.ulisboa.pt

Instituto Superior Técnico, Lisboa, Portugal

October 2018

Abstract

An Inertial Navigation System is a good solution for short missions. However, it suffers from open-loop integration problems of the sensors' noise and bias. Circumventing these problems involves considering additional sensors. A common solution used is a satellite-based navigation device, such as the Global Positioning System (GPS). In underwater navigation, the GPS is unavailable due to high attenuation. Therefore, other devices must be considered, where acoustic navigation systems are common solutions. In this thesis, a navigation system aided by an acoustic positioning system in a long baseline configuration is considered. A model for the system is devised, including a bias added to the ranges measured, which accounts for the effect of the unknown offset between the emitters' and receivers' clocks. The proposed solutions, which estimate the position, velocity, gravity acceleration, and bias of the vehicle, are the Extended Kalman Filter (EKF), the Unscented Kalman Filter (UKF), and a Linear Kalman Filter (LKF) derived after state augmentation. The EKF and UKF lack global convergence guarantees. The observability analysis performed for the LKF allows to establish globally exponentially stable error dynamics. The LKF and EKF have similar processing times, whereas the UKF has higher processing time. Monte Carlo simulations allow to conclude that the LKF presents smaller errors and Root-mean-square Error (RMSE) than the other proposed solutions. Therefore, the novel navigation solution is better than the typical estimation methods, removing also the burden of clock synchronization.

Keywords: underwater navigation systems, LBL, INS, clock synchronization, pseudo-range

1. Introduction

1.1. An introduction to underwater navigation systems

Accurate navigation systems are essential for the successful operation of autonomous and non-autonomous vehicles, providing navigation data that is useful, whether for geo-referencing, guidance, or for control purposes. Most navigation systems contain an Inertial Navigation System (INS), which uses data obtained from the sensors of an Inertial Measurement Unit (IMU). While the INS is self-contained, and offers good performance for short missions, it suffers from problems with open-loop integration of both the sensors' noise and bias. Over time, the open-loop integration increases the errors in states of interest, such as the heading and position of the vehicle, as evidenced in [14]. Circumventing these problems involves implementing sensor fusion, i.e., coupling the INS with additional sensors, which, although not inertial, allow the design of observers or filters that correct the estimation error via feedback.

Underwater navigation systems are of great importance, being used by divers, and Unmanned Underwater Vehicles (UUV) such as Autonomous Underwater Vehicles (AUV), and Remotely operated underwater vehicle (ROV). Unlike Global Positioning System (GPS) signals and most radio signals, acoustic waves aren't quickly absorbed and propagate far underwater and at a measurable rate, allowing to measure the distance between a receiver and one or a series of transponders, as seen in [8]. Acoustic navigation systems are generally categorized into three broad classes: Long Baseline (LBL), Short Baseline (SBL), and Ultra Short Baseline (USBL).

While harder to install, LBL systems have the highest accuracy among the acoustic positioning methods. The baseline transponders are installed in the work reference site, and the geometry of the baseline transponders network is favorable for position estimation. Furthermore, it operates fully underwater, which proves to be convenient in situations where the sea surface is far from the work site. A GPS Intelligent Buoy (GIB) can also be

deployed for high accuracy if the work site is sufficiently close to the surface, although not always being the case. Therefore, an LBL system is chosen to aid the INS in this thesis.

1.2. Clock synchronization problem

An acoustic navigation system relies on measuring distances based on the travel time of an acoustic signal. In one-way-travel-time mode, the travel time is computed as the difference between the time that the signal was emitted and the time that it was received. Therefore, there are measurement errors associated to the differences between the time in the emitter's and the receivers' clocks. Even if initially set to the same time, the rate that the clocks count time is different and will create, over time, a clock drift. Therefore, clock synchronization is important to accurately measure ranges, that is, to minimize the bias in the pseudo-ranges from the offset between the receiver's and emitters' clocks.

1.3. Problem addressed and proposed solutions

The main objective of this thesis is the development of a novel navigation system for LBL navigation aided by an IMU and an Attitude and Heading Reference System (AHRS), that includes the estimation of a bias, considered to be constant, which accounts for the effect of the unknown offset between the clocks of the emitters and the receivers. Therefore, the burden of initial clock synchronization is removed. The pseudo-ranges measured from the sensors consist of range measurements corrupted by an additive constant factor. These low-rate measurements allow to decrease the estimation error to values close to zero, using feedback, whereas the higher rate AHRS and IMU measurements, drive the vehicle dynamics and are integrated in open-loop. A dynamic non-linear model of the system, using pseudo-ranges, is derived and used in the observer design.

The estimation solutions available to solve the problem proposed are the Extended Kalman Filter (EKF), the Unscented Kalman Filter (UKF), and a Linear Kalman Filter (LKF) derived after system augmentation. The EKF is a common solution to navigation problems, where a general application that presents the algorithm used in this thesis is in [7]. The UKF algorithm used is presented in [13]. System state augmentation [1] will be performed, considering the LBL configuration, allowing to design an augmented system that can be regarded as linear for observability analysis and observer design purposes. Observability analysis will then be performed in order to design an observer that conveys globally exponentially stable error dynamics.

Monte Carlo simulations are one of the best tools to compare the solutions, allowing to compute errors and root-mean-square error (RMSE) averaged over a significant number of simulations, computed for each instant of time. With the obtained results, one can easily draw conclusions to the relative performance of the solutions devised, by analyzing the evolution of the errors and RMSE, as well as computing the mean error and RMSE over time, for each algorithm.

Other underwater navigation systems besides acoustic have been recently studied, with the first example being sonar imaging localization, as seen in [4]. While localization using Light-emitting diode (LED) has been studied for scenarios on land, as seen in [15], and [5], LED underwater localization is a recent topic of studies, as evidenced in [10] and will experience developments in the coming years. Simultaneous localization and mapping (SLAM), specially useful in AUV, consists of a machine mapping the environment and localizing itself in this environment, and has been an active topic of research. SLAM techniques, although out of this thesis' scope, could be applied to the acoustic navigation algorithms presented. AUV navigation, localization, and challenges faced, can be seen in [9], where camera-based localization is also discussed.

1.4. Organization of the thesis

The organization of the thesis is the following. Problem statement and notation are introduced in Section 2. The solutions proposed, namely, EKF, LKF, and UKF, are presented, respectively, in Sections 3, 4, and 5. Further analysis using Monte Carlo simulations is performed in Chapter 6.

2. Problem Statement and Notation

2.1. Notation

Throughout the dissertation, scalars, vectors and matrices are represented by a lowercase letter, a bold lowercase letter, and a bold uppercase letter, respectively. The symbol $\mathbf{0}_{n\times m}$ denotes a $n \times m$ matrix of zeros, $\mathbf{I}_n$ an identity matrix with dimension $n \times n$, and $\mathbf{diag}(\mathbf{A}_1, \ldots, \mathbf{A}_n)$ a block diagonal matrix. When the matrix dimensions are omitted, the matrices are assumed of appropriate dimensions. Given two vectors $\mathbf{x} \in \mathbb{R}^3$ and $\mathbf{y} \in \mathbb{R}^3$, $\mathbf{x} \times \mathbf{y}$ and $\mathbf{x} \cdot \mathbf{y}$ represent, respectively, the cross and inner products.

2.2. Problem Statement

Consider an underwater vehicle moving in a scenario where a set of landmarks with fixed and available positions are disposed in a LBL configuration. The landmarks are beacons that emit a signal tagged with the senders' time, which is then received by the acoustic receiver installed on the vehicle. Typically, the clock of the receiver is synchronized with the clock of the senders and the distance measured is obtained from the time-of-flight and sound speed profile. In this thesis, it is con-

sidered that there is an offset between the emitting and receiver clocks, assumed to be an unknown constant. As such, instead of range measurements, one has pseudo-range measurements, obtained periodically. Further suppose that the vehicle is equipped with an IMU, consisting of two triads of orthogonally mounted accelerometers and rate gyros and an AHRS. Figure 1 depicts the aforementioned scenario.

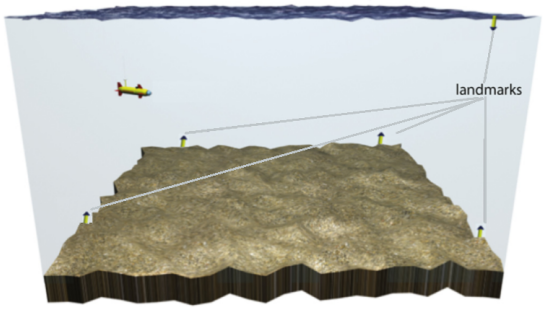

Figure 1: Underwater LBL scenario (Adapted from Batista, 2009 [3])

2.2.1 System Dynamics

Let {I} denote a local inertial reference frame, such as the North-East-Down (NED) frame, and {B} a body-fixed reference frame. The linear motion of the vehicle respects

$$\dot{\mathbf{p}}(t) = \mathbf{R}(t)\mathbf{v}(t), \tag{1}$$

where $\mathbf{p}(t) \in \mathbb{R}^3$ is the inertial position of the vehicle, $\mathbf{v}(t) \in \mathbb{R}^3$ is the velocity of the vehicle relative to the reference frame {I} expressed in the body-fixed reference frame {B}, and $\mathbf{R}(t)$ is the rotation matrix from the reference frame {B} to {I}, which satisfies $\dot{\mathbf{R}}(t) = \mathbf{R}(t)\mathbf{S}(\boldsymbol{\omega}(t))$, where $\boldsymbol{\omega}(t) \in \mathbb{R}^3$ is the angular velocity of the vehicle expressed in the reference frame {B} and $\mathbf{S}(\boldsymbol{\omega}(t))$ is the skew-symmetric matrix such that $\mathbf{S}(\boldsymbol{\omega}(t))\mathbf{x} = \boldsymbol{\omega} \times \mathbf{x}$. The rotation matrix $\mathbf{R}(t)$ and the angular velocity $\boldsymbol{\omega}(t)$ are provided by the AHRS. The IMU, which is assumed to be located at the center of mass of the vehicle, measures the linear acceleration $\mathbf{a}(t)$, given by

$$\mathbf{a}(t) = \dot{\mathbf{v}}(t) + \mathbf{S}(\boldsymbol{\omega}(t))\mathbf{v}(t) - \mathbf{g}(t), \tag{2}$$

where $\mathbf{g}(t) \in \mathbb{R}^3$ denotes the acceleration of gravity expressed in the reference frame {B}. This term must be considered due to the inherent physics of non-ideal accelerometers, see [6] for further details. It would be possible to cancel out this term in (2), since the magnitude of $\mathbf{g}(t)$ is usually well-known. However, since even small errors on the rotation matrix $\mathbf{R}(t)$ would lead to large errors in the estimated acceleration, the acceleration of gravity is considered to be an unknown state such as $\mathbf{p}(t)$ and $\mathbf{v}(t)$. The term $\mathbf{S}(\boldsymbol{\omega}(t))\mathbf{v}(t)$ represents the Coriolis acceleration and cannot be neglected, especially for vehicles executing aggressive maneuvers. Finally, given the positions $\mathbf{s}_i \in \mathbb{R}^3, i = 1, \ldots, n_L$, of the landmarks, let $b_c(t)$ be the bias term that accounts for the effect of the unknown offset of the clocks between the emitters and receivers. The pseudo-range measurements are given by

$$r_i(k) = \|\mathbf{s}_i - \mathbf{p}(t_k)\| + b_c(t_k), \tag{3}$$

with $t_k := t_0 + kT, k \in \mathbb{N}$, where $T > 0$ is the sampling period and t_0 is the initial time. The following assumptions are considered.

Assumption 1. The pseudo-range measurements are positive, i.e., $r_i(k) > 0, \forall k, i = 1, \ldots, L$.

Assumption 2. The offset of the clocks between the emitters and the receiver is constant, i.e., $\dot{b}_c(t) = 0$.

The derivative of the acceleration of gravity is considered to be constant in inertial coordinates, which gives

$$\dot{\mathbf{g}}(t) = -\mathbf{S}(\boldsymbol{\omega}(t))\mathbf{g}(t). \tag{4}$$

Combining (1) and (3) to (4), as well as Assumption 2, yields the nonlinear system

$$\begin{cases} \dot{\mathbf{p}}(t) = \mathbf{R}(t)\mathbf{v}(t) \\ \dot{\mathbf{v}}(t) = \mathbf{a}(t) - \mathbf{S}(\boldsymbol{\omega}(t))\mathbf{v}(t) + \mathbf{g}(t) \\ \dot{\mathbf{g}}(t) = -\mathbf{S}(\boldsymbol{\omega}(t))\mathbf{g}(t) \\ \dot{b}_c(t) = 0 \\ r_1(k) = \|\mathbf{s}_1 - \mathbf{p}(t_k)\| + b_c(t_k) \\ \vdots \\ r_L(k) = \|\mathbf{s}_L - \mathbf{p}(t_k)\| + b_c(t_k) \end{cases}. \tag{5}$$

The problem addressed in this thesis is the design of estimation solutions for (5).

In the accelerometer measurements (2), accelerometer bias was not considered. For the sake of simplicity and clarity of presentation, the accelerometer is assumed to be calibrated.

2.2.2 Long Baseline Configuration

The LBL configuration has been widely used in the past in the design of navigation systems. In the remainder of the dissertation, the following assumption is made

Assumption 3. There exist at least 5 noncoplanar landmarks

In the case of at least 4 noncoplanar landmarks, it is possible to obtain the position of a vehicle from range measurements. Given that the measurements obtained from the sensors are corrupted with bias, which adds another variable to be estimated, an extra landmark is considered in order to guarantee a correct estimation. Although the assumption of having at least 5 available noncoplanar landmarks was performed, the proposed solutions, i.e., the algorithms used, are general, and can be employed for any given number of landmarks.

3. Extended Kalman filter

Let $\mathbf{T}(t) := \mathbf{diag}(\mathbf{I}, \mathbf{R}(t), \mathbf{R}(t), 1) \in \mathbb{R}^{10\times 10}$ be a Lyapunov state transformation, previously used in [2], and consider the state transformation

$$\begin{bmatrix}\mathbf{z}_1(t)\\ \mathbf{z}_2(t)\\ \mathbf{z}_3(t)\\ z_4(t)\end{bmatrix} := \mathbf{T}(t)\begin{bmatrix}\mathbf{p}(t)\\ \mathbf{v}(t)\\ \mathbf{g}(t)\\ b_c(t)\end{bmatrix}. \tag{6}$$

Then, the new system dynamics can be written as

$$\begin{cases}\dot{\mathbf{z}}_1(t) = \mathbf{z}_2(t)\\ \dot{\mathbf{z}}_2(t) = \mathbf{z}_3(t) + \mathbf{R}(t)\mathbf{a}(t)\\ \dot{\mathbf{z}}_3(t) = \mathbf{0}\\ \dot{z}_4(t) = 0\\ r_1(k) = \|\mathbf{s}_1 - \mathbf{z}_1(t_k)\| + z_4(t_k)\\ \vdots\\ r_L(k) = \|\mathbf{s}_L - \mathbf{z}_1(t_k)\| + z_4(t_k)\end{cases}. \tag{7}$$

As (6) is a Lyapunov transformation, all observability properties are preserved (see [2]). Implementing the state transformation (6) is advantageous as the new system (7), albeit still nonlinear, is now time invariant, considering $\mathbf{R}(t)\mathbf{a}(t)$ as an input. Considering only the first four states, exact discretization is performed, which yields

$$\begin{cases}\mathbf{z}_1(t_{k+1}) = \mathbf{z}_1(t_k) + T\mathbf{z}_2(t_k) + \frac{T^2}{2}\mathbf{z}_3(t_k) + \\ \qquad + \int_{t_k}^{t_{k+1}} (t_{k+1}-\tau)\mathbf{R}(\tau)\mathbf{a}(\tau)d\tau\\ \mathbf{z}_2(t_{k+1}) = \mathbf{z}_2(t_k) + T\mathbf{z}_3(t_k) + \\ \qquad + \int_{t_k}^{t_{k+1}} \mathbf{R}(\tau)\mathbf{a}(\tau)d\tau\\ \mathbf{z}_3(t_{k+1}) = \mathbf{z}_3(t_k)\\ z_4(t_{k+1}) = z_4(t_k)\end{cases}, \tag{8}$$

Inverting the Lyapunov transformation, in discrete-time, gives

$$\mathbf{T}^{-1}(t_k) = \mathbf{diag}(\mathbf{I}, \mathbf{R}^T(t_k), \mathbf{R}^T(t_k), 1),$$

since the rotation matrix is orthonormal, i.e. $\mathbf{R}^{-1}(t) = \mathbf{R}^T(t)$. This transformation can then be applied to (6) and discrete-time states can be defined, that is,

$$\begin{bmatrix}\mathbf{x}_1(k)\\ \mathbf{x}_2(k)\\ \mathbf{x}_3(k)\\ x_4(k)\end{bmatrix} := \begin{bmatrix}\mathbf{p}(t_k)\\ \mathbf{v}(t_k)\\ \mathbf{g}(t_k)\\ b_c(t_k)\end{bmatrix} := \mathbf{T}^{-1}(t_k)\begin{bmatrix}\mathbf{z}_1(t_k)\\ \mathbf{z}_2(t_k)\\ \mathbf{z}_3(t_k)\\ z_4(t_k)\end{bmatrix}.$$

The discrete-time system dynamics, after re-introducing the pseudo-range measurements, can be written as

$$\begin{cases}\mathbf{x}_1(k+1) = \mathbf{x}_1(k)\\ \qquad + T\mathbf{R}(t_k)\mathbf{x}_2(k) + \frac{T^2}{2}\mathbf{R}(t_k)\mathbf{x}_3(k)\\ \qquad + \mathbf{u}_1(k)\\ \mathbf{x}_2(k+1) = \mathbf{R}^T(t_{k+1})\mathbf{R}(t_k)\mathbf{x}_2(k)\\ \qquad + T\mathbf{R}^T(t_{k+1})\mathbf{R}(t_k)\mathbf{x}_3(k) + \mathbf{u}_2(k)\\ \mathbf{x}_3(k+1) = \mathbf{R}^T(t_{k+1})\mathbf{R}(t_k)\mathbf{x}_3(k)\\ x_4(k+1) = x_4(k)\\ r_1(k) = \|\mathbf{s}_1 - \mathbf{x}_1(k)\| + x_4(k)\\ \vdots\\ r_L(k) = \|\mathbf{s}_L - \mathbf{x}_1(k)\| + x_4(k)\end{cases}, \tag{9}$$

where

$$\mathbf{u}_1(k) = \int_{t_k}^{t_{k+1}} (t_{k+1}-\tau)\mathbf{R}(\tau)\mathbf{a}(\tau)d\tau \tag{10}$$

and

$$\mathbf{u}_2(k) = \mathbf{R}^T(t_{k+1})\int_{t_k}^{t_{k+1}} \mathbf{R}(\tau)\mathbf{a}(\tau)d\tau. \tag{11}$$

The implementation of a EKF to (9) is standard, see [7].

4. Augmented states system and LKF

This section presents the steps taken to design a filter that yields globally exponentially stable error dynamics. State augmentation is performed in Section 4.1 and observability analysis is described in Section 4.2.

4.1. State Augmentation

As a function of the system states in (9), the pseudo-ranges are given by

$$r_i(k) = \|\mathbf{s}_i - \mathbf{x}_1(k)\| + x_4(k), \quad i = 1, \ldots, L.$$

To encode the LBL structure, the difference of pseudo-ranges to different beacons is computed (refer to full version of the thesis), and can be expressed as

$$\begin{aligned} r_i(k) - r_j(k) = &-2\frac{\mathbf{s}_i - \mathbf{s}_j}{r_i(k) + r_j(k)} \cdot \mathbf{x}_1(k) + \\ &+ 2\frac{r_i(k) - r_j(k)}{r_i(k) + r_j(k)}x_4(k) + \frac{\|\mathbf{s}_i\|^2 - \|\mathbf{s}_j\|^2}{r_i(k) + r_j(k)} \end{aligned}, \tag{12}$$

for $i, j \in \{1, \ldots, L\}, i \neq j$. This approach is similar to the one presented in [1], albeit with different state transition equations. These differences are defined as new states,

$$\begin{bmatrix} x_5(k) \\ x_6(k) \\ \vdots \\ x_{3+C_2^L}(k) \\ x_{4+C_2^L}(k) \end{bmatrix} := \begin{bmatrix} r_1(k) - r_2(k) \\ r_1(k) - r_3(k) \\ \vdots \\ r_{L-2}(k) - r_L(k) \\ r_{L-1}(k) - r_L(k) \end{bmatrix},$$

where C_2^L is the number of 2-combinations for a set of L elements, i.e., $C_2^L = \frac{L(L-1)}{2}$. Further computation is performed, showing that the dynamics of the new states can be written as

$$\begin{aligned}
[r_i(k+1) - r_j(k+1)] &= \frac{-2(\mathbf{s}_i - \mathbf{s}_j)^T T \mathbf{R}(t_k)}{r_i(k+1) + r_j(k+1)} \mathbf{x}_2(k) \\
&+ \frac{-(\mathbf{s}_i - \mathbf{s}_j)^T T^2 \mathbf{R}(t_k)}{r_i(k+1) + r_j(k+1)} \mathbf{x}_3(k) \\
&+ \frac{2\left[(r_i(k+1) - r_i(k)) - (r_j(k+1) - r_j(k))\right]}{r_i(k+1) + r_j(k+1)} x_4(k) \\
&+ \frac{r_i(k) + r_j(k)}{r_i(k+1) + r_j(k+1)} \left[r_i(k) - r_j(k)\right] \\
&+ \frac{-2(\mathbf{s}_i - \mathbf{s}_j)^T}{r_i(k+1) + r_j(k+1)} \mathbf{u}_1(k)
\end{aligned} \tag{13}$$

The augmented state vector is then defined as

$$\mathbf{x}(k) := \begin{bmatrix} \mathbf{x}_1(k) \\ \mathbf{x}_2(k) \\ \mathbf{x}_3(k) \\ x_4(k) \\ x_5(k) \\ \vdots \\ x_{4+C_2^L}(k) \end{bmatrix} \in \mathbb{R}^{10+C_2^L}. \tag{14}$$

The state dynamic equation for the augmented state vector can then be written, in compact form, as

$$\mathbf{x}(k+1) = \mathbf{A}(k)\mathbf{x}(k) + \mathbf{B}\mathbf{u}_a(k),$$

where $\mathbf{A}(k) \in \mathbb{R}^{(10+C_2^L)\times(10+C_2^L)}$ is defined as

$$\mathbf{A}(k) = \begin{bmatrix} \mathbf{A}_{11}(k) & \mathbf{0}_{10\times C_2^L} \\ \mathbf{A}_{21}(k) & \mathbf{A}_{22}(k) \end{bmatrix},$$

with $\mathbf{A}_{11}(k) \in \mathbb{R}^{10\times 10}$, $\mathbf{A}_{21}(k) \in \mathbb{R}^{C_2^L \times 10}$ and $\mathbf{A}_{22}(k) \in \mathbb{R}^{C_2^L \times C_2^L}$, $\mathbf{B} \in \mathbb{R}^{(10+C_2^L)\times(6+C_2^L)}$ given by

$$\mathbf{A}_{11}(k) = \mathbf{F}(k) = \begin{bmatrix} \mathbf{I} & T\mathbf{R}(t_k) & \frac{T^2}{2}\mathbf{R}(t_k) & \mathbf{0}_{3\times 1} \\ \mathbf{0}_3 & \mathbf{R}^T(t_{k+1})\mathbf{R}(t_k) & T\mathbf{R}^T(t_{k+1})\mathbf{R}(t_k) & \mathbf{0}_{3\times 1} \\ \mathbf{0}_3 & \mathbf{0}_3 & \mathbf{R}^T(t_{k+1})\mathbf{R}(t_k) & \mathbf{0}_{3\times 1} \\ \mathbf{0}_{1\times 3} & \mathbf{0}_{1\times 3} & \mathbf{0}_{1\times 3} & 1 \end{bmatrix},$$

$$\mathbf{A}_{21}(k) = \begin{bmatrix} \mathbf{0}_{1\times 3} & \frac{-2(\mathbf{s}_1-\mathbf{s}_2)^T T\mathbf{R}(t_k)}{r_1(k+1)+r_2(k+1)} & \frac{-(\mathbf{s}_1-\mathbf{s}_2)^T T^2\mathbf{R}(t_k)}{r_1(k+1)+r_2(k+1)} \\ \mathbf{0}_{1\times 3} & \frac{-2(\mathbf{s}_1-\mathbf{s}_3)^T T\mathbf{R}(t_k)}{r_1(k+1)+r_3(k+1)} & \frac{-(\mathbf{s}_1-\mathbf{s}_3)^T T^2\mathbf{R}(t_k)}{r_1(k+1)+r_3(k+1)} \\ \vdots & \vdots & \vdots \\ \mathbf{0}_{1\times 3} & \frac{-2(\mathbf{s}_{L-2}-\mathbf{s}_L)^T T\mathbf{R}(t_k)}{r_{L-2}(k+1)+r_L(k+1)} & \frac{-(\mathbf{s}_{L-2}-\mathbf{s}_L)^T T^2\mathbf{R}(t_k)}{r_{L-2}(k+1)+r_L(k+1)} \\ \mathbf{0}_{1\times 3} & \frac{-2(\mathbf{s}_{L-1}-\mathbf{s}_L)^T T\mathbf{R}(t_k)}{r_{L-1}(k+1)+r_L(k+1)} & \frac{-(\mathbf{s}_{L-1}-\mathbf{s}_L)^T T^2\mathbf{R}(t_k)}{r_{L-1}(k+1)+r_L(k+1)} \end{bmatrix},$$

$$\begin{bmatrix} \frac{2[(r_1(k+1)-r_1(k))-(r_2(k+1)-r_2(k))]}{r_1(k+1)+r_2(k+1)} \\ \frac{2[(r_1(k+1)-r_1(k))-(r_3(k+1)-r_3(k))]}{r_1(k+1)+r_3(k+1)} \\ \vdots \\ \frac{2[(r_{L-2}(k+1)-r_{L-2}(k))-(r_L(k+1)-r_L(k))]}{r_{L-2}(k+1)+r_L(k+1)} \\ \frac{2[(r_{L-1}(k+1)-r_{L-1}(k))-(r_L(k+1)-r_L(k))]}{r_{L-1}(k+1)+r_L(k+1)} \end{bmatrix}$$

$$\begin{aligned}
\mathbf{A}_{22}(k) = \mathbf{diag}\Bigg(& \frac{r_1(k) + r_2(k)}{r_1(k+1) + r_2(k+1)}, \\
& \frac{r_1(k) + r_3(k)}{r_1(k+1) + r_3(k+1)}, \ldots, \\
& \frac{r_{L-2}(k) + r_L(k)}{r_{L-2}(k+1) + r_L(k+1)}, \\
& \frac{r_{L-1}(k) + r_L(k)}{r_{L-1}(k+1) + r_L(k+1)} \Bigg)
\end{aligned},$$

$$\mathbf{B} = \begin{bmatrix} \mathbf{I}_3 & \mathbf{0}_3 & \mathbf{0}_{3\times C_2^L} \\ \mathbf{0}_3 & \mathbf{I}_3 & \mathbf{0}_{3\times C_2^L} \\ \mathbf{0}_3 & \mathbf{0}_3 & \mathbf{0}_{3\times C_2^L} \\ \mathbf{0}_{1\times 3} & \mathbf{0}_{1\times 3} & \mathbf{0}_{1\times C_2^L} \\ \mathbf{0}_{C_2^L\times 3} & \mathbf{0}_{C_2^L\times 3} & \mathbf{I}_{C_2^L} \end{bmatrix},$$

and

$$\mathbf{u}_a(k) = \begin{bmatrix} \mathbf{u}_1(k) \\ \mathbf{u}_2(k) \\ \frac{-2(\mathbf{s}_1-\mathbf{s}_2)^T}{r_1(k+1)+r_2(k+1)}\mathbf{u}_1(k) \\ \frac{-2(\mathbf{s}_1-\mathbf{s}_3)^T}{r_1(k+1)+r_3(k+1)}\mathbf{u}_1(k) \\ \vdots \\ \frac{-2(\mathbf{s}_{L-2}-\mathbf{s}_L)^T}{r_{L-2}(k+1)+r_L(k+1)}\mathbf{u}_1(k) \\ \frac{-2(\mathbf{s}_{L-1}-\mathbf{s}_L)^T}{r_{L-1}(k+1)+r_L(k+1)}\mathbf{u}_1(k) \end{bmatrix} \in \mathbb{R}^{6+C_2^L}.$$

Discarding the original nonlinear output, noticing that the states $x_5(k), \ldots x_{4+C_2^L}(k)$ are available and using (12), one may write the augmented discrete-time system, in compact form

$$\begin{cases} \mathbf{x}(k+1) = \mathbf{A}(k)\mathbf{x}(k) + \mathbf{B}\mathbf{u}_a(k) \\ \mathbf{y}(k+1) = \mathbf{C}(k+1)\mathbf{x}(k+1) \end{cases}, \tag{15}$$

where $\mathbf{C}(k) \in \mathbb{R}^{2C_2^L \times (10+C_2^L)}$ is defined as

$$\mathbf{C}(k) = \begin{bmatrix} \mathbf{0} & \mathbf{0} & \mathbf{0} & \mathbf{0}_{3\times 1} & \mathbf{I} \\ \mathbf{C}_{21}(k) & \mathbf{0} & \mathbf{0} & \mathbf{C}_{24}(k) & \mathbf{I} \end{bmatrix}$$

with $\mathbf{C}_{21}(k) \in \mathbb{R}^{L\times 3}$ and $\mathbf{C}_{24}(k) \in \mathbb{R}^{L}$ given by

$$\mathbf{C}_{21}(k) = \begin{bmatrix} 2\frac{(\mathbf{s}_1-\mathbf{s}_2)^T}{r_1(k)+r_2(k)} \\ 2\frac{(\mathbf{s}_1-\mathbf{s}_3)^T}{r_1(k)+r_3(k)} \\ \vdots \\ 2\frac{(\mathbf{s}_{L-2}-\mathbf{s}_L)^T}{r_{L-2}(k)+r_L(k)} \\ 2\frac{(\mathbf{s}_{L-1}-\mathbf{s}_L)^T}{r_{L-1}(k)+r_L(k)} \end{bmatrix},$$

and

$$\mathbf{C}_{24}(k) = \begin{bmatrix} -2\frac{r_1(k)-r_2(k)}{r_1(k)+r_2(k)} \\ -2\frac{r_1(k)-r_3(k)}{r_1(k)+r_3(k)} \\ \vdots \\ -2\frac{r_{L-2}(k)-r_L(k)}{r_{L-2}(k)+r_L(k)} \\ -2\frac{r_{L-1}(k)-r_L(k)}{r_{L-1}(k)+r_L(k)} \end{bmatrix}.$$

Notice that $\mathbf{C}_{21}(k)$ and $\mathbf{C}_{24}(k)$ were defined to encode (12).

4.2. Observability Analysis

The discrete time-varying system (15) can still be considered linear in the state for observer design purposes, even though the system matrices $\mathbf{A}(k)$ and $\mathbf{C}(k)$ depend on the pseudo-range measurements. This is possible because the pseudo-range measurements are assumed to be available, and therefore are considered as functions of time for observer (or filter) design purposes.

Theorem 1 and Theorem 2 address, respectively, the observability of the discrete-time system (15) and the observability of the non-linear system (9).

Theorem 1. Suppose that the LBL acoustic configuration is such that, for some $k_i \geq k_0$, the matrix

$$\mathbf{L}(k_i) = \begin{bmatrix} (\mathbf{s}_1-\mathbf{s}_2)^T & -[r_1(k_i)-r_2(k_i)] \\ (\mathbf{s}_1-\mathbf{s}_3)^T & -[r_1(k_i)-r_3(k_i)] \\ \vdots & \vdots \\ (\mathbf{s}_{L-2}-\mathbf{s}_L)^T & -[r_{L-2}(k_i)-r_L(k_i)] \\ (\mathbf{s}_{L-1}-\mathbf{s}_L)^T & -[r_{L-1}(k_i)-r_L(k_i)] \end{bmatrix}$$

is full rank, i.e.,

$$rank(\mathbf{L}(k_i)) = 4. \tag{16}$$

Then, the discrete-time system is observable on the interval $[k_i, k_i+3]$ in the sense that the initial state $\mathbf{x}(k_i)$ is uniquely determined by the input $\{\mathbf{u}(k) : k = k_i, k_i+1, k_i+2\}$ and the output $\{\mathbf{y}(k) : k = k_i, k_i+1, k_i+2\}$.

Proof. The proof reduces to demonstrating that the observability matrix $\mathcal{O}(k_i, k_i+3)$ associated with the pair $(\mathbf{A}(k), \mathbf{C}(k))$ on $[k_i, k_i+3], k_i \geq k_0$ has rank equal to the number of states of the system (refer to complete version of the thesis).

Theorem 2. Suppose that (16) holds for some $k_i \geq k_0$. Then:

1. the nonlinear system (9) is observable on the interval $[k_i, k_i+3]$ in the sense that the initial state $x(k_i)$ is uniquely determined by the input $\{\mathbf{u}(k) : k = k_i, k_i+1, k_i+2\}$ and the output $\{\mathbf{y}(k) : k = k_i, k_i+1, k_i+2\}$.
2. the initial condition of the augmented system (15) matches that of the nonlinear system (9) on the interval $[k_i, k_i+3]$, i.e.,

$$\begin{cases} \mathbf{x}_1(k_i) = \mathbf{p}(t_{k_i}) \\ \mathbf{x}_2(k_i) = \mathbf{v}(t_{k_i}) \\ \mathbf{x}_3(k_i) = \mathbf{g}(t_{k_i}) \\ x_4(k_i) = b_c(t_{k_i}) \\ x_5(k_i) = \|\mathbf{s}_1 - \mathbf{p}(t_{k_i})\| - \|\mathbf{s}_2 - \mathbf{p}(t_{k_i})\| \\ x_6(k_i) = \|\mathbf{s}_1 - \mathbf{p}(t_{k_i})\| - \|\mathbf{s}_3 - \mathbf{p}(t_{k_i})\| \\ \vdots \\ x_{3+C_2^L}(k_i) = \|\mathbf{s}_{L-2} - \mathbf{p}(t_{k_i})\| - \|\mathbf{s}_L - \mathbf{p}(t_{k_i})\| \\ x_{4+C_2^L}(k_i) = \|\mathbf{s}_{L-1} - \mathbf{p}(t_{k_i})\| - \|\mathbf{s}_L - \mathbf{p}(t_{k_i})\| \end{cases}.$$

Proof. The proof is done by showing that the initial condition of (9) corresponds to that of (15), in the conditions of the theorem. Since using Theorem 1 allows to conclude that the initial condition of (15) is uniquely determined and the two initial conditions from both systems match, it follows that the initial condition of (9) is also uniquely determined.

4.3. Globally exponentially stable error dynamics

Although the EKF and UKF correctly estimate the variables of interest, i.e., were able to minimize the estimation error to a value close to zero, there are initial conditions with which the error does not converge to zero. Choosing the initial conditions as, for example, $\mathbf{x}_1(0) = [-3000 \quad -3000 \quad 1000]^T[m]$, $\mathbf{x}_2(0) = [100 \quad 100 \quad 100]^T[m/s]$, $\mathbf{x}_3(0) = [1000 \quad 1000 \quad 1000]^T[m/s^2]$, and $x_4(0) = -500\ m$, the result obtained (presented in the full version) allows to conclude that the position estimation does not converge with this initial condition for both the filters. The LKF has been proven to have globally exponentially stable error dynamics, in Section 4.2, and given the same initial condition, this estimation error converges to zero.

5. Unscented Kalman filter

The proposed EKF filter approximates the nonlinear observation model through a first-order linearization, assuming that the state distribution is approximated by a Gaussian random variable. This can introduce errors that influence the posterior mean and covariance of the state distribution, which may lead to the filter having a sub-optimal performance. The UKF addresses this problem by representing the state distribution using a set of care-

fully chosen points, that attempt to capture the mean and covariance of the state distribution more accurately than the EKF. These points are called *sigma* points and, when propagated through the non-linear system, yield a posterior mean and covariance of the state distribution closer to its real value [13].

6. Monte Carlo Simulations

6.1. Setup

In order to evaluate the performance achieved by the proposed navigation algorithms, numerical simulations were performed. Even though the full non-linear dynamics of the vehicle are not considered, the proposed filter still applies to any underwater vehicle since it relies solely on the vehicle kinematics, which are exact.

The vehicle described the trajectory shown in Fig. 2. The initial position is $\mathbf{p}_0 = [150 \quad 150 \quad 70]^T(m)$, whereas the body-fixed velocity was assumed to be constant $\mathbf{v}(t) = [1 \quad 0 \quad 0]^T(m/s)$, and the bias that accounts for the effect of the clocks offset was defined to be 50 m.

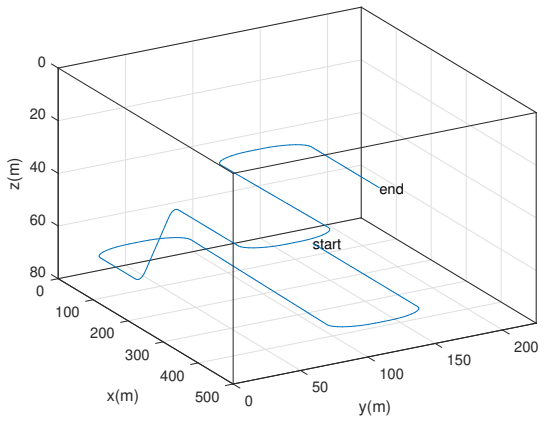

Figure 2: Trajectory described by the underwater vehicle

The AHRS and IMU provide measurements with a frequency of 10 Hz, while the pseudo-range measurements have a sample time of 5 s. Sensor noise was considered in all sensors. The pseudo-range, acceleration and angular velocity are assumed to be corrupted by zero-mean white Gaussian noise, with standard deviations of 1 m, 2×10^{-3} m/s^2 and 0.05^o $/s$, respectively. The attitude which was parameterized by roll, pitch and yaw Euler angles, was assumed to be corrupted by zero-mean white Gaussian noise, with standard deviation of 0.03 ^{o} for the roll and pitch and 0.3 ^{o} for the yaw. The LBL configuration is composed of 5 beacons, with known positions,

$$\mathbf{s}_1 = \begin{bmatrix} 0 \\ 1000 \\ 0 \end{bmatrix}(m), \mathbf{s}_2 = \begin{bmatrix} 0 \\ 1000 \\ 1000 \end{bmatrix}(m), \mathbf{s}_3 = \begin{bmatrix} 1000 \\ 0 \\ 750 \end{bmatrix}(m),$$

$$\mathbf{s}_4 = \begin{bmatrix} 0 \\ 0 \\ 500 \end{bmatrix}(m), \mathbf{s}_5 = \begin{bmatrix} 250 \\ 0 \\ 250 \end{bmatrix}(m).$$

The measurements provided by the AHRS and IMU measurements are obtained at a higher frequency than the pseudo-range measurements. Therefore, the open-loop integration can be performed at a higher frequency, between pseudo-range measurements, as given by

$$\begin{cases} \mathbf{p}(t) = \mathbf{p}(t_k) + (t-t_k)\mathbf{R}(t_k)\mathbf{v}(t_k) + \\ \qquad + \dfrac{(t-t_k)^2}{2}\mathbf{R}(t_k)\mathbf{g}(t_k) \\ \qquad + \displaystyle\int_{t_k}^{t}(t-\tau)\mathbf{R}(\tau)\mathbf{a}(\tau)d\tau \\ \mathbf{v}(t) = \mathbf{R}^T(t)\mathbf{R}(t_k)\mathbf{v}(t_k) \\ \qquad + (t-t_k)\mathbf{R}^T(t)\mathbf{R}(t_k)\mathbf{g}(t_k) + \\ \qquad + \mathbf{R}^T(t)\displaystyle\int_{t_k}^{t}\mathbf{R}(\tau)\mathbf{a}(\tau)d\tau \\ \mathbf{g}(t) = \mathbf{R}^T(t)\mathbf{R}(t_k)\mathbf{g}(t_k) \\ b_c(t) = b_c(t_k) \end{cases} . \quad (17)$$

To tune the Kalman filters, the system was simulated in open-loop to evaluate the state disturbance driven by the sensor noise, that is, at every instant, the system was run in open-loop starting from the real value of the states until the next sampled time. Then, for each state computed from the exact value, the corresponding error was calculated, which provided an approximation for the state disturbance intensity matrix. The state disturbance intensity matrix was then set to $\mathbf{Q} = \mathbf{diag}(10^{-3}\mathbf{I}, 10^{-4}\mathbf{I}, 10^{-5}\mathbf{I}, 10^{-1})$ and the output noise intensity matrix was chosen as $\mathbf{R} = \mathbf{I}$. The initial conditions were set to zero for the position and velocity. The initial estimate of the acceleration of gravity was set close to its true value, with $[0 \quad 0 \quad 10]^T(m/s^2)$, since the attitude is measured and the magnitude of the acceleration of gravity is usually known. Notice that it would be possible to initialize the position and clocks offset with a close estimate obtained from the inversion of the first set of LBL range measurements.

The Kalman filter for the augmented system (LKF) was tuned, with a state disturbance covariance matrix set to $\mathbf{Q}_a = \mathbf{diag}(\mathbf{Q}, \mathbf{I})$ and a output noise covariance matrix set to $\mathbf{R}_a = \mathbf{diag}(\mathbf{R}, 2\mathbf{I})$. The initial guess of the augmented states was obtained by the corresponding difference between initial pseudo-ranges.

For each algorithm described above, 1000 simulations of 1200 seconds were performed and the initial estimate $\mathbf{x}_0$ was set to the true value $\mathbf{x}_{0_{true}}$ with an added variable $\Delta\mathbf{x}$, which can be written as

$$\mathbf{x}_0 = \mathbf{x}_{0_{true}} + \Delta\mathbf{x}, \tag{18}$$

where $\Delta\mathbf{x}$ is a zero-mean Gaussian variable with standard deviation of $\sigma_p = 100m$ for the position, $\sigma_v = 0.2m/s$ for the velocity, $\sigma_g = 0.01m/s^2$ for the gravity acceleration, and $\sigma_{b_c} = 10m$ for the bias representing the clocks offset. The initial covariance $\mathbf{P}_0$ was set accordingly, written as

$$\mathbf{P}_0 = \begin{bmatrix} \sigma_p\mathbf{I}_3 & \mathbf{0} & \mathbf{0} & \mathbf{0} \\ \mathbf{0} & \sigma_v\mathbf{I}_3 & \mathbf{0} & \mathbf{0} \\ \mathbf{0} & \mathbf{0} & \sigma_g\mathbf{I}_3 & \mathbf{0} \\ \mathbf{0} & \mathbf{0} & \mathbf{0} & \sigma_{b_c} \end{bmatrix}. \tag{19}$$

The error is computed for each simulation and each sample. From these values, one extracts the mean-error for each sampled time, and the RMSE for each sampled time, which is then compared to the Bayesian Cramér-Rao Bound (BCRB) obtained in Section 6.2. For sake of brevity and because the conclusion obtained for the initial convergence and detailed evolution are similar, only the former is shown here.

6.2. Bayesian Cramér-Rao Bound

The BCRB is a lower bound on the mean squared estimation error. Therefore, it is a useful reference to evaluate the performance of each algorithm. A recursive BCRB is derived in [12], for the case of a linear Gaussian process model and a nonlinear observation model with Additive white Gaussian noise (AWGN). The recursion can be written as

$$\begin{aligned} \mathbf{J}(k+1) = &\left[\mathbf{Q} + \mathbf{F}(k)\mathbf{J}_n^{-1}\mathbf{F}(k)^T\right]^{-1} \\ &+ E_{\mathbf{x}(k+1)}\left\{\tilde{\mathbf{H}}^T(k+1)\mathbf{R}^{-1}\tilde{\mathbf{H}}(k+1)\right\}, \end{aligned} \tag{20}$$

where $\mathbf{J}(k+1)$ is the BCRB, $\mathbf{Q}$ is the state disturbance intensity matrix which was already defined, $\mathbf{F}(k)$ is the state transition matrix, $\mathbf{H}(k)$ is a linear estimation of the observation model state matrix and $\mathbf{R}$ is the output noise intensity matrix, which was also already defined. The BCRB was calculated using the true state values $\mathbf{x}_{true}$ for each sampled time.

6.3. Initial convergence

The initial convergence of both the mean-error and the RMSE of the position, velocity, and gravity acceleration were similar for the three components of each state of interest. Therefore, and for the sake of brevity, only the mean-error and RMSE of the x-component of each state are represented, for the LKF, EKF, and UKF.

The initial convergence of the mean-error for the position $p_x(t)$, velocity $v_x(t)$, gravity acceleration $g_x(t)$, and bias $b_c(t)$, is represented, respectively, in Figs. 3, 5, 7, and 9. From these figures, one can conclude that the LKF presents a much faster convergence than the EKF and UKF. The UKF estimation mean-error shows the biggest overshoot, followed by the EKF and LKF.

The initial convergence of the RMSE for the position $p_x(t)$, velocity $v_x(t)$, gravity acceleration $g_x(t)$, and bias $b_c(t)$, is represented, respectively, in Figs. 4, 6, 8, and 10. The convergence time is similar to the one for the mean-error, with the LKF showing a much faster transient period.

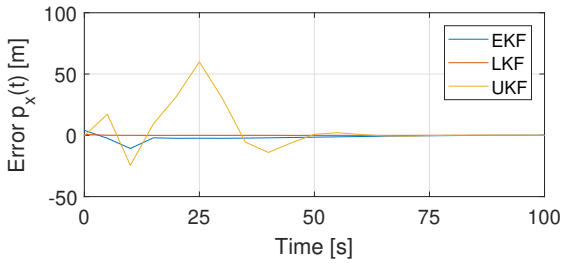

Figure 3: Initial convergence of the position $p_x(t)$ mean-error for each algorithm

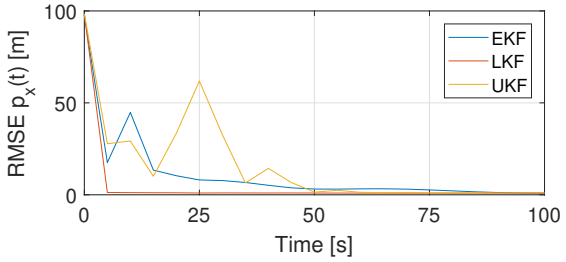

Figure 4: Initial convergence of the position $p_x(t)$ RMSE for each algorithm

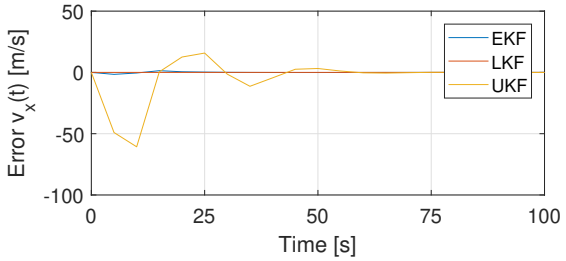

Figure 5: Initial convergence of the velocity $v_x(t)$ mean-error for each algorithm

6.4. Average mean-error and average RMSE vs processing time

From the initial convergence and detailed evolution (refer to full version of thesis) of each variable of interest, it is possible to draw the conclusion that the LKF is the best filter in this case, showing no overshoot, which was observed for the EKF, and the UKF. The LKF also has a faster convergence time. Adding to its advantages are the guarantee of globally exponentially stable error dynamics.

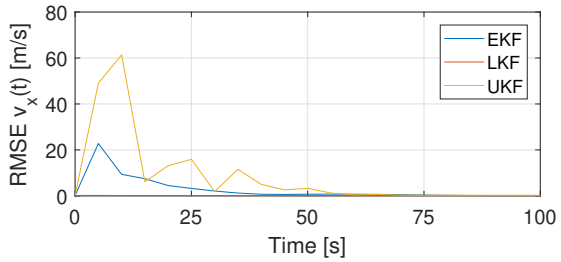

Figure 6: Initial convergence of the velocity $v_x(t)$ RMSE for each algorithm

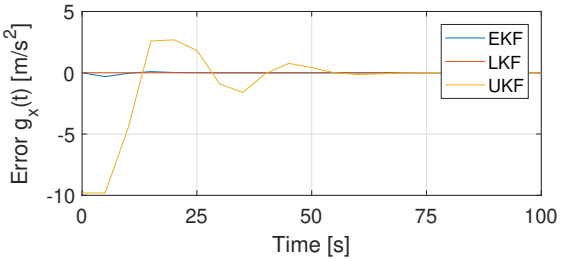

Figure 7: Initial convergence of the gravity acceleration $g_x(t)$ mean-error for each algorithm

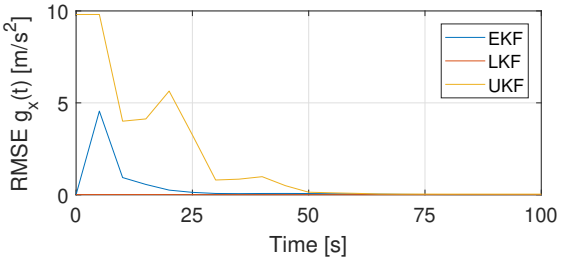

Figure 8: Initial convergence of the gravity acceleration $g_x(t)$ RMSE for each algorithm

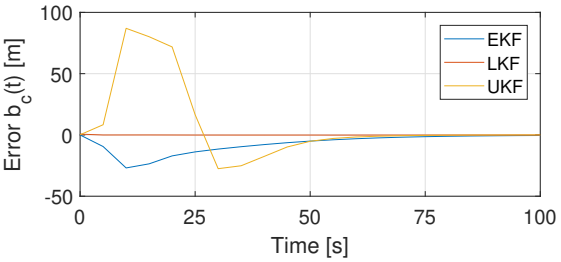

Figure 9: Initial convergence of the bias $b_c(t)$ mean-error for each algorithm

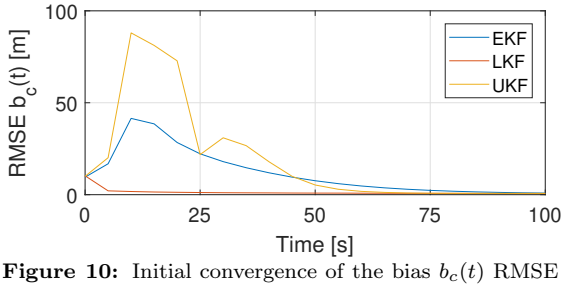

Figure 10: Initial convergence of the bias $b_c(t)$ RMSE for each algorithm

Tables 1 and 2 show the average mean-error for the x-coordinate of the position, velocity, and gravity acceleration, and the bias, for each algorithm. It can be observed that the LKF presents small average mean-errors, similar to the UKF and smaller than the EKF. The same can be concluded from the analysis of Tables 3 and 4, where the UKF shows the worst results in this case.

The processing time was calculated and presented (refer to full version of the thesis), allowing to conclude that the LKF and EKF are the fastest algorithms, with the UKF being 1.5 times slower.

Mean error	$p_x\ (m)$	$v_x\ (m/s)$
EKF	-8.9×10^{-2}	-1.0×10^{-3}
LKF	-2.4×10^{-2}	-4.5×10^{-5}
UKF	1.2×10^{-2}	9.4×10^{-5}

Table 1: Average mean-error for the position and velocity for each algorithm

Mean error	$g_x\ (m/s^2)$	$b_c\ (m)$
EKF	1.6×10^{-4}	2.2×10^{-1}
LKF	-6.1×10^{-6}	-5.8×10^{-2}
UKF	4.3×10^{-5}	3.1×10^{-2}

Table 2: Average mean-error for the gravity acceleration and bias for each algorithm

RMSE	p_x	v_x
EKF	7.8×10^{-1}	6.4×10^{-2}
LKF	9.0×10^{-1}	8.9×10^{-2}
UKF	1.0×10^{0}	2.6×10^{-1}

Table 3: Average RMSE for the position and velocity for each algorithm

RMSE	g_x	$b_c\ (m)$
EKF	5.8×10^{-3}	5.5×10^{-1}
LKF	6.8×10^{-3}	6.1×10^{-1}
UKF	3.6×10^{-2}	7.2×10^{-1}

Table 4: Average RMSE for the gravity acceleration and bias for each algorithm

7. Conclusions

The problem approached was to design a novel navigation system in a LBL configuration, aided by an IMU and an AHRS which removes the burden of synchronization by estimating a bias that accounts for the offset between the clocks of the emitters and receivers. The objective was accomplished, with different solutions implemented, that is, the EKF, UKF, and LKF with system augmentation.

To compare these solutions, Monte Carlo simulations were performed, with each algorithm being run in the same conditions. The BCRB computed was lower than the RMSE for each pair of state of interest and algorithm used.

The UKF and EKF can be shown to not converge under specific initial conditions. Monte Carlo simulations evidenced that the performance of the EKF is better than the one of the UKF, with smaller stationary errors and RMSE for each state as well as a faster convergence time. The estimation time for the UKF is also, roughly, 1.5 times bigger than the one for the EKF. Therefore, one can conclude that the EKF is a better solution than the UKF.

The simulations for the solution with the EKF and LKF show similar errors and RMSE in stationary state and in the same order of magnitude, with the LKF having a faster convergence time and globally exponentially stable error dynamics, as demonstrated in its corresponding observability analysis. Therefore, the LKF is evidently superior to the EKF, as well as the UKF.

It should be noted that the solution devised could be implemented for a navigation system over water, as long as a LBL configuration is present, since acoustic waves can travel at a measurable/estimable rate in this environment. The algorithm can also be implemented with GIB, where the position of the landmarks constantly changes during estimation, according to the position obtained from the GPS sensors in each buoy.

A conference article [11] that presents the problem statement, and observer design, as well as some simulation results obtained, will be submitted to the European Control Conference, as well as an extended version of it, in a scientific journal, with Monte Carlo simulations and comparison to the BCRB, EKF and UKF.

References

[1] P. Batista. Long baseline navigation with clock offset estimation and discrete-time measurements. *Control Engineering Practice*, 35:43–53, 2015.

[2] P. Batista, C. Silvestre, and P. Oliveira. Position and velocity optimal sensor-based navigation filters for UAVs. In *Proceedings of the American Control Conference*, pages 5404–5409, 2009.

[3] P. Batista, C. Silvestre, and P. Oliveira. On the Observability of Linear Motion Quantities in Navigation Systems. In *Systems & Control Letters*, volume 60, pages 665–673, 2011.

[4] H. Johannsson, M. Kaess, B. Englot, F. Hover, and J. Leonard. Imaging sonar-aided navigation for autonomous underwater harbor surveillance. *IEEE/RSJ 2010 International Conference on Intelligent Robots and Systems, IROS 2010 - Conference Proceedings*, pages 4396–4403, 2010.

[5] S. Y. Jung, S. Hann, and C. S. Park. TDOA-based optical wireless indoor localization using LED ceiling lamps. *IEEE Transactions on Consumer Electronics*, 57(4):1592–1597, 2011.

[6] A. Kelly. Modern Inertial and Satellite Navigation Systems, 1994.

[7] Y.-R. Kim, S.-K. Sul, and M.-H. Park. Speed sensorless vector control of induction motor using extended Kalman filter. *IEEE Transactions on Industry Applications*, 30(5):1225–1233, 1994.

[8] P. H. Milne. *Underwater Acoustic Positioning Systems*. Gulf Publishing Company, 1983.

[9] L. Paull, S. Saeedi, M. Seto, and H. Li. AUV navigation and localization: A review. *IEEE Journal of Oceanic Engineering*, 39(1):131–149, 2014.

[10] S. C. Shen, C. J. Chen, H. J. Huang, and C. Pan. Evaluation of MEMS inertial sensor module for underwater vehicle navigation application. *2010 International Conference on Mechanic Automation and Control Engineering*, pages 3807–3810, 2010.

[11] T. Silva and P. Batista. GES INS-aided Long Baseline Navigation with clock offset estimation and discrete-time measurements. *to be submitted to European Control Conference*.

[12] B. K. Trees H. *Bayesian Bounds for Parameter Estimation and Nonlinear Filtering/Tracking*. Wiley, 2007.

[13] E. A. Wan and R. Van Der Merwe. The unscented Kalman filter for nonlinear estimation. In *Technology*, volume v, pages 153–158. Proceedings of the IEEE 2000 Adaptive Systems for Signal Processing, Communications, and Control Symposium, 2000.

[14] O. J. Woodman. An introduction to inertial navigation. Technical Report 696, University of Cambridge, 2007.

[15] W. Zhang and M. Kavehrad. A 2-D indoor localization system based on visible light LED. *2012 IEEE Photonics Society Summer Topical Meeting Series, PSST 2012*, 4:80–81, 2012.